PAPER • **OPEN ACCESS**

Thick interface size effect on dislocation transmission in nanolaminates

To cite this article: S Xu *et al* 2022 *IOP Conf. Ser.: Mater. Sci. Eng.* **1249** 012005

Thick interface size effect on dislocation transmission in nanolaminates

S Xu[1,*], J Y Cheng[2], N A Mara[2] and I J Beyerlein[1,3]

[1] Department of Mechanical Engineering, University of California, Santa Barbara, California 93106-5070, USA
[2] Department of Chemical Engineering and Materials Science, University of Minnesota, Minneapolis, MN 55455, USA
[3] Materials Department, University of California, Santa Barbara, California 93106-5050, USA

E-mail: shuozhixu@ucsb.edu

Abstract.
Recent experimental studies have reported that thick interfaces in nanolaminates can lead to greater strengths than conventionally sharp interfaces without sacrificing deformability. Using a multi-phase phase-field dislocation dynamics model, dislocation transmission across a compositionally graded, nanoscale thick interface is investigated. Thicker interfaces over a finite range are found to lead to greater resistance to transmission. The limit interface thickness at which the peak resistance is reached, and the strengthening capacity of the interface are greater when the dislocation is dissociated, as in a face-centered cubic lattice, than when it is compact, as in a body-centered cubic lattice. The composition transitions within the interface are treated with multiple sublayers, and it is found that the interface transmission barrier is as strong as its most resistance composition.

1. Introduction

Nanolaminates have drawn considerable attention due to their extraordinarily high strength, beyond the volume averaged strength based on their constituents [1, 2]. They consist of a stack of alternating layers of two or more dissimilar materials, wherein the individual layer thicknesses are nanoscale in dimension. Their superior strength, as well as many other notable properties, such as outstanding thermal stability [3], good room temperature ductility [4, 5], and excellent shock resistance [6, 7], have been attributed to their high density of interfaces. Interfaces in conventional face-centered cubic (FCC)/body-centered cubic (BCC) nanolaminates are sharp, composed of one atomic plane of Cu and one atomic plane of Nb [8]. In 2018, Chen et al. [9] synthesized Cu/Nb nanolaminates with interfaces that were on the contrary thick. As shown in figure 1, these thick Cu/Nb interfaces extend out of plane by at least a few nm and are chemically, crystallographically, and/or topologically distinct from those of the Cu or Nb crystals they join. Compression testing 40 nm/40 nm Cu/Nb nanolaminates revealed that when the interface thickness is about 10 nm, the yield stress is 50% higher and the flow stress 22% higher than when the interface is sharp, while retaining the same strain to failure of 14%. Another study revealed that even higher strengths and deformability were possible when both the interface and layer thicknesses equaled 10 nm [10]. Clearly, these thick or so-called 3D interfaces introduce newer and more variables to interface design than the commonly studied sharp or 2D interfaces.

In this work, we use a recently developed multi-phase phase field dislocation dynamics (PFDD) model [11] to investigate the role of 3D interface thickness h' and composition on the critical stress for dislocation transmission.

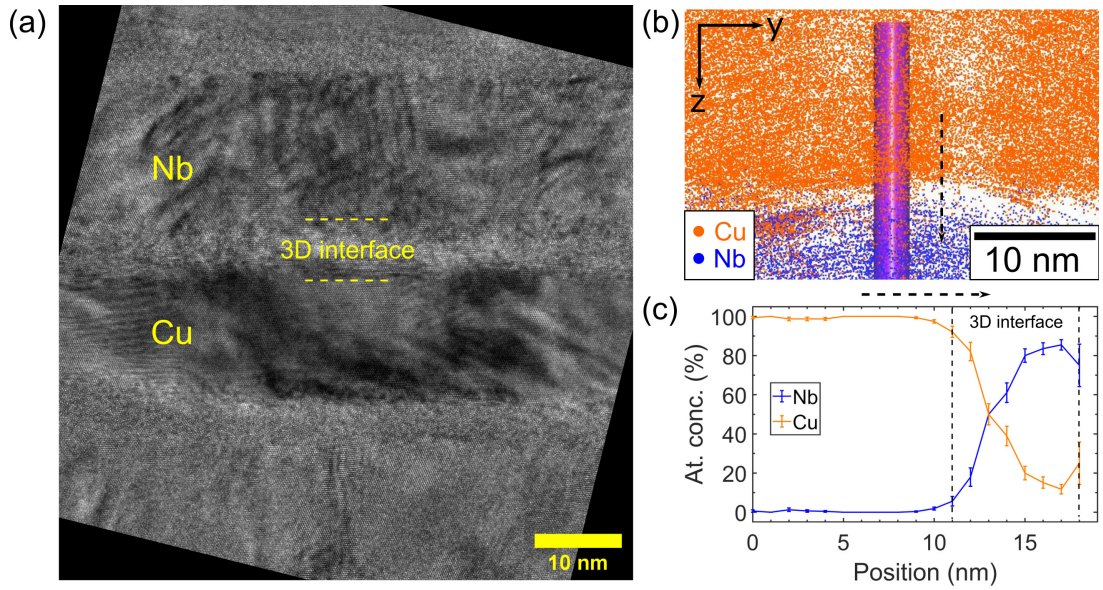

Figure 1. (a) A high-resolution transmission electron micrograph of a 3D Cu-Nb interface between a Cu layer and a Nb layer. More details were presented in Ref. [10]. (b) An atom probe tomography chemical map of the 3D interface. The purple cylinder represents a region of interest from which the line profile of chemical composition in (c) is extracted. The horizontal dashed arrow indicates the directionality in (b) and the two vertical dotted lines correspond to the two horizontal yellow lines in (a). More details were presented in Ref. [12].

2. Methods

2.1. PFDD formulation

In the formulation, each phase field order parameter is associated with an available slip system. Accordingly, the set of order parameters $\boldsymbol{\phi}$ consists of n_{op} order parameters, for which there are N_{sp} slip planes and n_{sp} slip directions per slip plane. Thus, $n_{\text{op}} = N_{\text{sp}} n_{\text{sp}}$. The order parameter for a given slip system α, denoted by ϕ_α, is 0 for the unslipped state and 1 or more for the slipped state. The total system energy consists of energetic terms that are a function of the evolving order parameters [13]. For a multi-phase material, a second quantity, a virtual strain tensor $\boldsymbol{\epsilon}^{\text{v}}$ independent of $\boldsymbol{\phi}$, is introduced and included in the solution [11].

The total energy density ψ at a given material point $\boldsymbol{x}$ contains the elastic ψ_{ela}, lattice ψ_{lat}, gradient ψ_{gra}, and external ψ_{ext} energy densities [14],

$$\psi(\boldsymbol{x}) = \psi_{\text{ela}}(\boldsymbol{x}) + \psi_{\text{lat}}(\boldsymbol{x}) + \psi_{\text{gra}}(\boldsymbol{x}) - \psi_{\text{ext}}(\boldsymbol{x}) \tag{1}$$

where ψ_{lat} and ψ_{gra} only exist in materials that contain dislocations.

The first energy density, ψ_{ela}, consists of two terms, the "equivalent" homogeneous elastic energy density, $\psi_{\text{ela}}^{\text{eq}}(\boldsymbol{x})$, and the "extra" elastic energy density, $\psi_{\text{ela}}^{\text{ex}}(\boldsymbol{x})$ [15], i.e.,

$$\psi_{\text{ela}}(\boldsymbol{x}) = \psi_{\text{ela}}^{\text{eq}}(\boldsymbol{x}) + \psi_{\text{ela}}^{\text{ex}}(\boldsymbol{x}) \tag{2}$$

$$\psi_{\text{ela}}^{\text{eq}}(\boldsymbol{x}) = \frac{1}{2}[\boldsymbol{\epsilon}(\boldsymbol{x}) - \boldsymbol{\epsilon}^0(\boldsymbol{x})] \cdot \boldsymbol{C}[\boldsymbol{\epsilon}(\boldsymbol{x}) - \boldsymbol{\epsilon}^0(\boldsymbol{x})] \tag{3}$$

$$\psi_{\text{ela}}^{\text{ex}}(\boldsymbol{x}) = \frac{1}{2}\boldsymbol{\epsilon}^{\text{v}}(\boldsymbol{x}) \cdot \boldsymbol{M}^{[N]}(\boldsymbol{x})\boldsymbol{\epsilon}^{\text{v}}(\boldsymbol{x}) \tag{4}$$

where $\boldsymbol{C}$ is the elasticity tensor and $\boldsymbol{\epsilon}$ the strain tensor, given by $\boldsymbol{\epsilon} = \operatorname{sym}\boldsymbol{\beta}$, where $\boldsymbol{\beta} = \nabla\boldsymbol{u}$ is the distortion with $\boldsymbol{u}$ the displacement in material N, $1 < N \leq N_{\text{mat}}$. $\psi_{\text{ela}}^{\text{ex}}$ exists in all materials except material $N = 1$. The eigenstrain tensor $\boldsymbol{\epsilon}^0$ depends on the material, according to

$$\boldsymbol{\epsilon}^0(\boldsymbol{x}) = \begin{cases} \boldsymbol{\epsilon}^{\text{p}}(\boldsymbol{x}), & \boldsymbol{x} \in \text{material 1} \\ \boldsymbol{\epsilon}^{\text{p}}(\boldsymbol{x}) + \boldsymbol{\epsilon}^{\text{v}}(\boldsymbol{x}), & \boldsymbol{x} \in \text{material } N \text{ where dislocations exist} \\ \boldsymbol{\epsilon}^{\text{v}}(\boldsymbol{x}), & \boldsymbol{x} \in \text{material } N \text{ where dislocations do not exist} \end{cases} \tag{5}$$

where $\boldsymbol{\epsilon}^{\text{p}}$ and $\boldsymbol{\epsilon}^{\text{v}}$ are the plastic strain tensor and virtual strain tensor, respectively. The tensor $\boldsymbol{\epsilon}^{\text{p}}$ is related to plastic distortion tensor $\boldsymbol{\beta}^{\text{p}}$ and order parameter $\boldsymbol{\phi}$ via

$$\boldsymbol{\epsilon}^{\text{p}} = \operatorname{sym}\boldsymbol{\beta}^{\text{p}} \tag{6}$$

$$\boldsymbol{\beta}^{\text{p}}(\boldsymbol{\phi}) = \sum_{\alpha=1}^{n_{\text{op}}} \frac{b_\alpha \phi_\alpha}{d_\alpha} \boldsymbol{s}_\alpha \otimes \boldsymbol{n}_\alpha \tag{7}$$

where $\boldsymbol{s}_\alpha$ is the slip direction unit vector, b_α is the slip vector magnitude, $\boldsymbol{n}_\alpha$ is the slip plane unit normal, and d_α is the interplanar distance for slip system α. In equation 4,

$$M_{ijkl}^{[N]}(\boldsymbol{x}) = -C_{ijmn}^{[1]} \left[\Delta C_{mnpq}^{[N]}(\boldsymbol{x})\right]^{-1} C_{pqkl}^{[1]} - C_{ijkl}^{[1]} \tag{8}$$

$$\Delta C_{ijkl}^{[N]}(\boldsymbol{x}) = C_{ijkl}^{[N]}(\boldsymbol{x}) - C_{ijkl}^{[1]} \tag{9}$$

The second energy density in equation 1, ψ_{lat}, is a function of $\boldsymbol{\phi}$ [16], i.e.,

$$\psi_{\text{lat}}(\boldsymbol{x}) = \frac{\gamma_{\text{gsf}}^{[N]}(\boldsymbol{\phi}(\boldsymbol{x}))}{l_{\text{gsf}}^{[N]}(\boldsymbol{x})} \tag{10}$$

where $\gamma_{\text{gsf}}^{[N]}$ is the generalized stacking fault energy (GSFE) and $l_{\text{gsf}}^{[N]}$ is the interplanar spacing for material N. For one system in the $\{110\}$ glide plane in the BCC lattice, $n_{\text{sp}} = 1$ and γ_{gsf} is represented by a GSFE curve along the $\langle 111 \rangle$ direction. For the FCC lattice, the three coplanar slip systems on the $\{111\}$ glide plane are used, and hence $n_{\text{sp}} = 3$ and γ_{gsf} is a GSFE surface.

The third energy density, ψ_{gra}, represents the energy associated with the change in $\boldsymbol{\phi}$ at the dislocation and hence is a function of the gradient $\nabla\phi_\alpha(\boldsymbol{x})$ [17]. It is related to the projection of the curl of the distortion tensor (Nye's tensor) in equation 7 onto each slip system as follows

$$\psi_{\text{gra}}(\boldsymbol{x}) = \sum_{\alpha,\beta=1}^{n_{\text{sp}}} \eta_{\alpha\beta}^{[N]} \nabla\phi_\alpha(\boldsymbol{x}) \cdot \boldsymbol{\Xi}_{\alpha\beta}(\boldsymbol{x}) \nabla\phi_\beta(\boldsymbol{x}) \tag{11}$$

where $\eta_{\alpha\beta}^{[N]}$ is a scaling factor for the gradient energy and has units of energy per unit length. It can be specified for a pair of order parameters $\alpha\beta$ in material N. The tensor $\boldsymbol{\Xi}_{\alpha\beta}$ depends on geometry and is:

$$\boldsymbol{\Xi}_{\alpha\beta} = \frac{\boldsymbol{b}_\alpha \cdot \boldsymbol{b}_\beta}{d_\alpha d_\beta}[(\boldsymbol{n}_\alpha \cdot \boldsymbol{n}_\beta)\boldsymbol{I} - \boldsymbol{n}_\beta \otimes \boldsymbol{n}_\alpha] \tag{12}$$

where $\boldsymbol{I}$ is the identity tensor. Here, for simplicity sake, we set $\eta_{\alpha\beta}^{[N]}$ the same for all $\alpha\beta$ pairs in the same material, and we drop the subscripts in what follows.

The last energy density in equation 1, the external energy density ψ_{ext}, is given by

$$\psi_{\text{ext}}(\boldsymbol{x}) = \boldsymbol{\sigma}_{\text{app}} \cdot \boldsymbol{\epsilon}^0(\boldsymbol{x}) \tag{13}$$

where $\boldsymbol{\sigma}_{\text{app}}$ is the applied stress tensor.

With the energy functional defined and order parameters initialized, the total system energy is minimized with respect to each order parameter ϕ_α and each virtual strain component ϵ_{ab} (where $a, b = 1, 2, 3$) via the time-dependent Ginzburg-Landau equations:

$$\dot{\phi}_\alpha(\boldsymbol{x}) = -m_0[\partial_{\phi_\alpha(\boldsymbol{x})}(\psi_{\text{ela}}(\boldsymbol{x}) + \psi_{\text{lat}}(\boldsymbol{x}) - \psi_{\text{ext}}(\boldsymbol{x})) - \nabla \cdot \partial_{\nabla\phi_\alpha(\boldsymbol{x})}\psi_{\text{gra}}(\boldsymbol{x})] \tag{14}$$

$$\dot{\epsilon}_{ab}^{\text{v}}(\boldsymbol{x}) = -m_0^{\text{v}}\partial_{\epsilon_{ab}^{\text{v}}(\boldsymbol{x})}(\psi_{\text{ela}}(\boldsymbol{x}) - \psi_{\text{ext}}(\boldsymbol{x})) \tag{15}$$

where the superposed dot denotes a time derivative. equation 15 is not applied to material 1. The Ginzburg-Landau coefficients, m_0 and m_0^{v}, are non-negative but not necessarily equal.

2.2. Simulation set-up

Figure 2 illustrates the 3D periodic simulation cell composed of an edge dislocation dipole bounded by a pair of 3D interfaces that lie perpendicular to the glide plane. To isolate the role of chemistry and interface thickness h', the two matrix crystals on either side of the interface belong to the same pure metal while the 3D interface consists of one or two Cu-Nb alloys with the same crystal structure as the matrix.

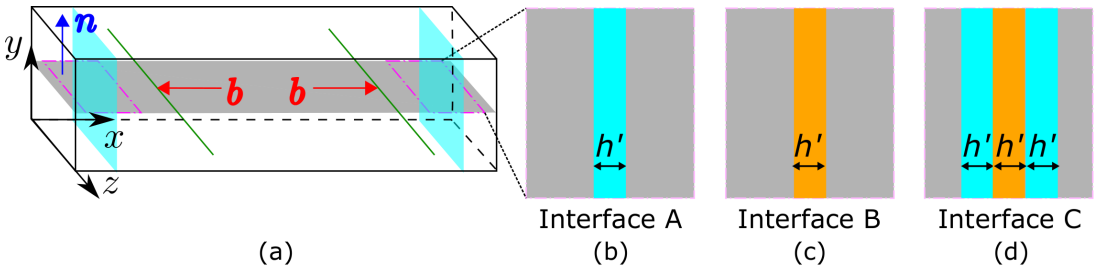

Figure 2. (a) Schematic of the simulation cell for an edge dislocation dipole interacting with two 3D interfaces in a Nb matrix or a Cu matrix. The grey parallelogram is the slip plane, while the interface plane normal is along the x axis. (b–d) In a Nb matrix, cyan and orange layers indicate BCC $Cu_{0.05}Nb_{0.95}$ (interface A) and BCC $Cu_{0.1}Nb_{0.9}$ (interface B), respectively; in a Cu matrix, cyan and orange layers correspond to FCC $Cu_{0.9}Nb_{0.1}$ (interface A) and FCC $Cu_{0.8}Nb_{0.2}$ (interface B), respectively.

For the BCC crystal, the glide plane is $\{110\}$ and the glide direction is $\langle 111\rangle$. The corresponding lattice orientations of the cell are

$$(\boldsymbol{i}_x, \boldsymbol{i}_y, \boldsymbol{i}_z) = \left(\frac{\sqrt{3}}{3}[111], \frac{\sqrt{2}}{2}[\bar{1}10], \frac{\sqrt{6}}{6}[\bar{1}\bar{1}2]\right) \tag{16}$$

For the FCC crystal, the slip system is $\{111\}\langle 110\rangle$ and the cell orientations are

$$(\boldsymbol{i}_x, \boldsymbol{i}_y, \boldsymbol{i}_z) = \left(\frac{\sqrt{2}}{2}[\bar{1}10], \frac{\sqrt{3}}{3}[111], \frac{\sqrt{6}}{6}[11\bar{2}]\right) \tag{17}$$

The lengths of the simulation cell, L_x, L_y, and L_z along the x, y, and z direction, respectively, are selected to minimize numerical artifacts. The number of grid points along the three directions, respectively, are 1024, 64, and 128. The two dislocations lie along the z axis on the mid-y plane, and are separated by $L_x/2$ along the x direction since this separation results in an equilibrium dipole position in its stress-free state. The two 3D interfaces are separated by $7L_x/8$ along the x direction. The distance between an interface and its adjacent dislocation is selected such that the two do not overlap even in the case of the thickest 3D interface studied (≈ 15 nm).

The interface composition is selected such that the interface would form a coherent, cube-on-cube orientation relationship with the adjoining matrix material. In a prior work, with some additional calculations from this work, atomistic calculations were conducted to determine the structure, lattice parameters, elastic moduli, and GSFEs for the full spectrum of Cu-Nb compositions [15]. They identify that $Cu_{0.05}Nb_{0.95}$ and $Cu_{0.1}Nb_{0.9}$ are stable BCC alloys while $Cu_{0.8}Nb_{0.2}$ and $Cu_{0.9}Nb_{0.1}$ stable FCC alloys. The other compositions, with intermediate Cu and Nb compositions, are amorphous materials and not considered here for the interface phase.

A compositionally graded 3D interface is modeled as a series of three layers, wherein the two outer layers bound to the matrix have the same composition, while the inner layer has a different composition. This transition intends to mimic the gradual composition transitions within the 3D interface seen in figure 1 [12]. Figure 2(d) shows this "trilayer" representation of a graded 3D interface, in which each layer thickness is h' and the total thickness is thus $3h'$. For the BCC case, the matrix is Nb and the interface transitions from $Cu_{0.05}Nb_{0.95}$ then $Cu_{0.1}Nb_{0.9}$ and back to $Cu_{0.05}Nb_{0.95}$ and Nb. Likewise, for the FCC case, the matrix is Cu and the trilayer interface is first $Cu_{0.9}Nb_{0.1}$ then $Cu_{0.8}Nb_{0.2}$, and returns to $Cu_{0.9}Nb_{0.1}$. The interface thickness $3h'$ varies from 1.71 nm ($5.94b_{\mathrm{Nb}}$) to 15.42 nm ($53.56b_{\mathrm{Nb}}$) in a Nb matrix, and from 1.53 nm ($5.95b_{\mathrm{Cu}}$) to 15.42 nm ($60.01b_{\mathrm{Cu}}$) in a Cu matrix.

For comparison, separate simulations are performed considering 3D interfaces but with a single alloy composition, as depicted in figure 2(b,c). When the matrix is Nb, the monolayer interface is either BCC $Cu_{0.05}Nb_{0.95}$ alloy or BCC $Cu_{0.1}Nb_{0.9}$ alloy. The thickness h' varies from 0.57 nm ($1.98b_{\mathrm{Nb}}$), approximately three times the inter-{111}-planar spacing, to 13.68 nm ($47.52b_{\mathrm{Nb}}$). When the matrix is Cu, the interfaces considered are either $Cu_{0.9}Nb_{0.1}$ or $Cu_{0.8}Nb_{0.2}$. The h' ranges from twice the inter-{110}-planar spacing, 0.51 nm ($1.98b_{\mathrm{Cu}}$) to 10.03 nm ($39.03b_{\mathrm{Cu}}$).

Table 1. Lattice parameters a_0 (in Å), elastic constants C_{11}, C_{12}, C_{44} (in GPa), isotropic shear modulus in Voigt form $\mu = (3C_{44} + C_{11} - C_{12})/5$, and uniform gradient energy coefficients η (in μb^2) of the two pure metals and four random binary alloys used in this work.

	Lattice	a_0	C_{11}	C_{12}	C_{44}	μ	η
Nb	BCC	3.324 [18]	245 [19]	132 [19]	28.4 [19]	39.64	0
$Cu_{0.05}Nb_{0.95}$	BCC	3.287	236.76	139	35.66	40.95	0
$Cu_{0.1}Nb_{0.9}$	BCC	3.274 [15]	221.58 [15]	141.63 [15]	40.63 [15]	40.37	0
$Cu_{0.8}Nb_{0.2}$	FCC	3.759 [15]	195.16 [15]	128.44 [15]	79.32 [15]	60.94	0.19 [11]
$Cu_{0.9}Nb_{0.1}$	FCC	3.699 [15]	187.25 [15]	135.8 [15]	81.88 [15]	59.42	0.28 [11]
Cu	FCC	3.634 [20]	169 [19]	122 [19]	75.3 [19]	54.58	0.38 [11]

Table 1 and Table 2 present the input parameters for every material and, when available, their originating references. The uniform gradient energy coefficient η scales directly with the size of the partial dislocation core, excluding the intrinsic stacking fault (ISF) [21]. For undissociated dislocations, such as those in BCC metals, the gradient term is neglected (i.e., $\eta = 0$). For the dissociated dislocations in FCC materials, η is characterized by comparisons with the partial

Table 2. Unstable stacking fault energy (SFE) γ_{usf} and intrinsic SFE γ_{isf} of the six materials in Table 1, in mJ/m^2.

	Nb	$Cu_{0.05}Nb_{0.95}$	$Cu_{0.1}Nb_{0.9}$	$Cu_{0.8}Nb_{0.2}$	$Cu_{0.9}Nb_{0.1}$	Cu
γ_{usf}	676.78 [18]	710.13	703.46 [15]	151.18 [15]	155.19 [15]	160.52 [20]
γ_{isf}				38.17 [15]	40.67 [15]	41.83 [20]

core widths in the same material based on atomistic simulations [11]. The boundaries between different materials are assumed coherent since the lattice misfit between any adjoining matrix and interface phase is sufficiently small. Further, any residual Burgers vector left after dislocation transmission would also be small and due to the appreciable thickness of the 3D interfaces, would be distributed across the interface thickness.

A resolved shear stress is applied to the system to drive the dislocations to glide towards the 3D interfaces. For FCC materials, the edge dislocation under no stress dissociates into leading and trailing Shockley partials. Under the stress applied here, the magnitude of the shear stress resolved on each partial is the same and drives them in the same direction. The applied stress is incremented in order to identify σ_c, the critical stress for the dislocation to transmit the entire thick interface. Specifically, when the minimum applied stress for transmission σ_0 is found, we set $\sigma_c = \sigma_0 - \Delta\sigma_0/2$, where $\Delta\sigma_0 = 10^{-4}\mu$ is the smallest difference between the two stresses and μ is the isotropic shear modulus of the matrix. For each stress level, the iterations performed to solve equation 15 are terminated when the Euclidean norm of the difference in global vector of each order parameter and each virtual strain component between successive iterations is smaller than 10^{-5}. The Ginzburg-Landau coefficients m_0 and m_0^{v} are set to unity and the timestep used is $\Delta t = 0.02$.

3. Results

3.1. Monolayer interface

Figure 3 presents σ_c for both interface compositions as a function of h' in the BCC case.

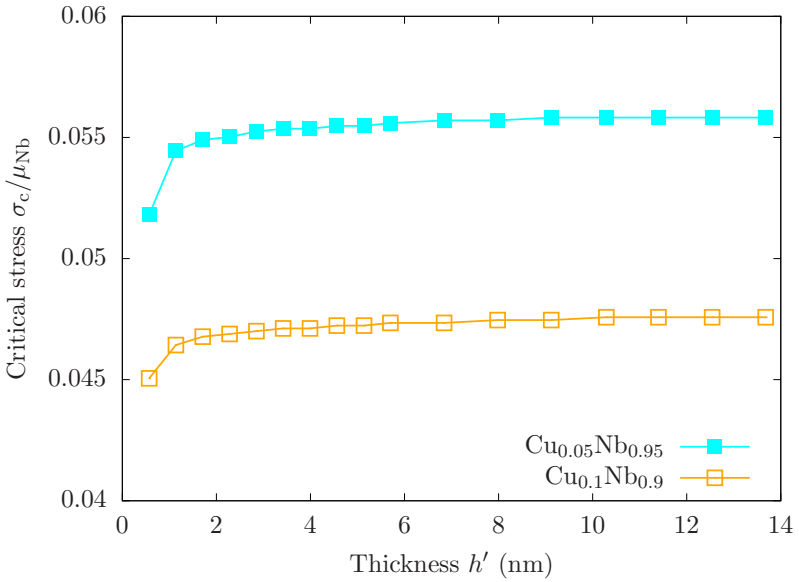

Figure 3. Critical stresses for transmission of an edge dislocation across thick interfaces in a Nb matrix, as a function of interface thickness.

Interfaces of any thickness substantially increase σ_c (30–60%) compared to the glide resistance in pure Nb, $0.033\mu_{Nb}$ (using the same model). The strengthening observed can be attributed to both higher μ and γ_{usf} of the interface. For the same h', the $Cu_{0.05}Nb_{0.95}$ interface composition, with the higher values of μ and γ_{usf}, provides the stronger barrier to transmission, than $Cu_{0.1}Nb_{0.9}$. The impact is large–with 4.8% higher γ_{usf} yielding on average 36% higher σ_c.

Importantly, thicker h' leads to higher σ_c. The positive size effect of h' on σ_c prevails, however, over a short range from 0.57 nm until $\approx$ 3 nm, beyond which there is no noticeable benefit to strengthening. The precise limit h' at which σ_c peaks is 9.12 nm for the $Cu_{0.05}Nb_{0.95}$ interface and 10.29 nm for the $Cu_{0.1}Nb_{0.9}$ one. Since σ_c is associated with a critical state of the dislocation, the locations of the dislocation in their sub-critical configurations are examined. Some configurations are shown in figure 4. They reveal that σ_c is needed to force transmission across the first boundary into the interface. For smaller h' where a positive size effect is seen, this first transmission event is aided by the image stresses from the interface boundary on the other side of the thick interface. For larger h', the aid diminishes and along with it, the size dependence.

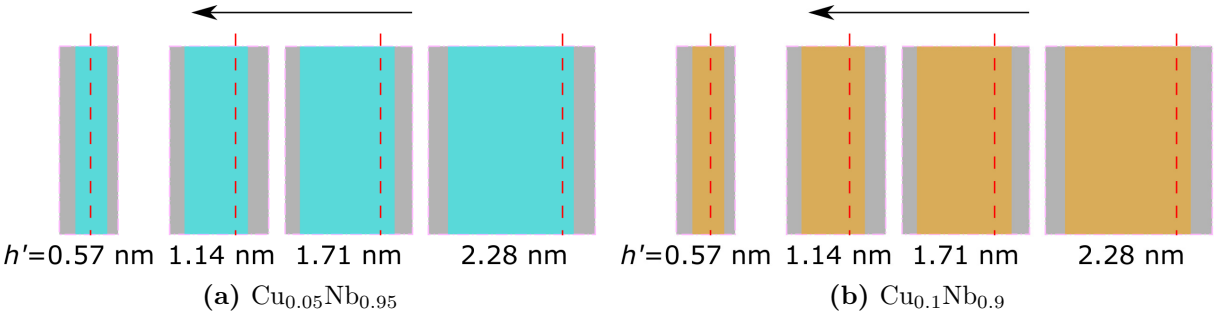

(a) $Cu_{0.05}Nb_{0.95}$ **(b)** $Cu_{0.1}Nb_{0.9}$

Figure 4. Position of the edge dislocation (vertical dashed line) with respect to the interface in a Nb matrix when the applied stress is slightly lower than the critical one. In each case, the dislocation moves from right to left, as indicated by the arrow. Partial views of the areas of interest are shown and do not represent the entire length of the simulation cell.

In the Cu matrix, introduction of a thick interface provides even greater increases in σ_c than in the Nb matrix. For comparison, the glide resistance for an edge dislocation in pure Cu using this model is $0.00035\mu_{Cu}$ [11]. As shown in figure 5, introduction of even the finest layer $\approx$ 0.6 nm increases σ_c at least 40 times. Further, unlike in the BCC case, the influence of 3D interface h' is strong and does not weaken until h' increases to around $\approx$ 4–5 nm. Between the two compositions, the $Cu_{0.9}Nb_{0.1}$ interface provides the greater transmission resistance than the $Cu_{0.8}Nb_{0.2}$ one, which would be expected since the former has the greater γ_{usf} and γ_{isf}.

The strengthening potential and strong size effect are counter-intuitive since transmitting and gliding across these interfaces from Cu would be expected to be easier than gliding in Cu alone since both interface compositions have a lower γ_{usf}, γ_{isf}, and their difference $\gamma_{usf} - \gamma_{isf}$ than pure Cu. It is also intriguing that the interfaces in the BCC counterpart did not provide strengthening to this extent although they have larger μ and γ_{usf} than the Nb matrix.

Analysis of sub-critical configurations in a Cu matrix suggests that the formation of the relatively low-energy ISF in the interface produces a strong pinning effect, that would not be realized in Nb. Figure 6 shows the positions of the leading (L) and trailing (T) partials in the sub-critical configurations, right before the pair (the full dislocation) completes transmission for a few h'. The L and T partials transmit across the first matrix/interface boundary and the interface thickness, maintaining approximately the same ISF width of $\approx$ 1.5–2 nm. This width is lower than the zero-stress ISF width in Cu, which is 2.53 nm ($= 9.85b_{Cu}$) and those in the alloys,

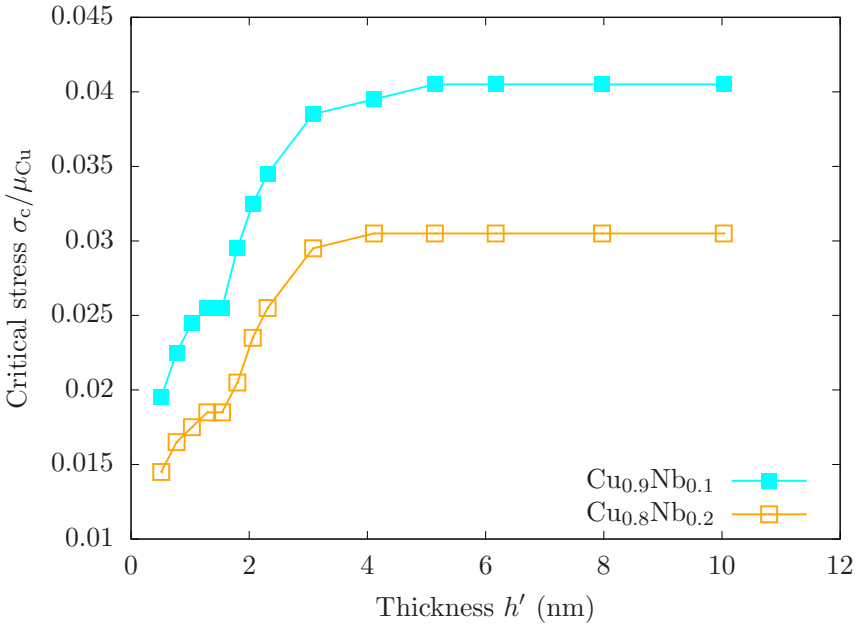

Figure 5. Critical stresses for transmission of an edge dislocation through two interface compositions in the Cu matrix, as a function of the interface thickness.

which are 2.59 nm and 2.63 nm, respectively [11]. For all thicknesses, the L partial transmits into the recipient Cu layer, while leaving the T partial in the interface and or the originating Cu layer. The σ_c is needed to push the T partial across the interface. As h' increases, the distance the L partial extends into Cu increases. The limit of h' is reached when the portion of the ISF width in the recipient Cu layer increases above that in the interface.

3.2. Trilayer interface

From the monolayer 3D interfaces, we turn our attention to the more compositionally complex trilayer interface, i.e., interface C in figure 2. We first consider the BCC case, in which the matrix is Nb and the interface transitions from $Cu_{0.1}Nb_{0.9}$ in the first outer layer adjacent to the Nb matrix to $Cu_{0.05}Nb_{0.95}$ in the central layer and back to $Cu_{0.1}Nb_{0.9}$ in the third layer. Figure 7 indicates that this gradient 3D interface of any thickness $3h'$ leads to an increase in σ_c above the Peierls stress in Nb, $0.03355\mu_{Nb}$ [15]. Importantly, these gradient interfaces have similar σ_c as the $Cu_{0.1}Nb_{0.9}$ monolayer interfaces for the same total thickness. Of the two compositions in the interface, $Cu_{0.05}Nb_{0.95}$ is the stronger one. An "inverse" weakest-link response is thus identified, wherein the barrier strength of the graded interface is as strong as its strongest composition.

Like the BCC monolayer interface, the size effect in $3h'$ on σ_c is positive for a short range until $\approx 3h' = 3.42$ nm when the size effect weakens and further increases in thickness produce little gain in barrier strength. For even greater $3h'$, a strict limit thickness is reached at which the peak σ_c is achieved. This limit $3h' = 10.26$ nm and is about three times the limit h' for either monolayer alloy interface. The locations of the dislocation at its critical point for a select set of $3h'$ are shown in figure 8a. In all cases, the critical stress is needed to force the dislocation to transmit across the first boundary into $Cu_{0.05}Nb_{0.95}$. Attaining this configuration is affected weakly by $3h'$. The limit $3h'$ is related to the distance beyond which the image stresses from the other boundaries become sufficiently minimized.

In a Cu matrix, the trilayer interface consists of two $Cu_{0.9}Nb_{0.1}$ layers adjacent to the matrix and one $Cu_{0.8}Nb_{0.2}$ layer in the middle. Like the monolayer interface, a strong size effect arises,

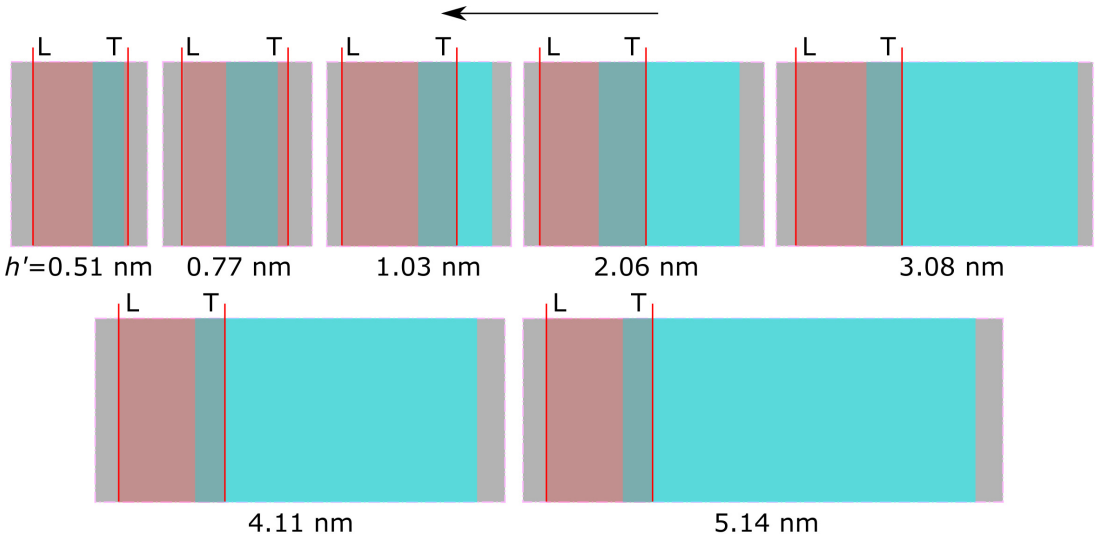

(a) $Cu_{0.9}Nb_{0.1}$

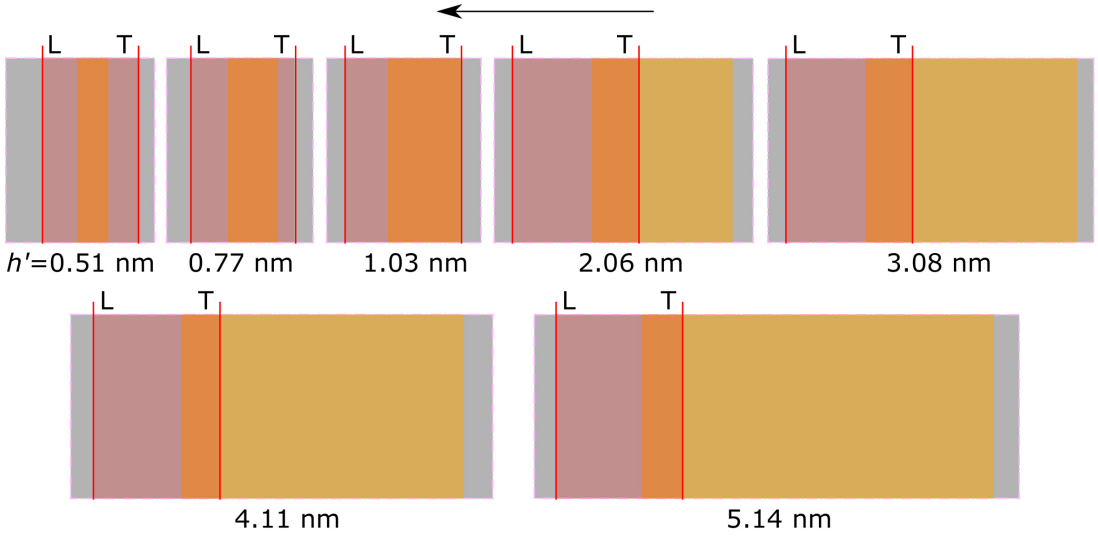

(b) $Cu_{0.8}Nb_{0.2}$

Figure 6. Position of the dissociated dislocation in its critical configuration in the Cu matrix when the applied stress is slightly lower than the critical one. Two Shockley partial dislocations are denoted by two vertical red lines, respectively, while the ISF by a semi-transparent red block between the two partials. "L" and "T" denote the leading and trailing partials, respectively.

as shown in figure 7, wherein σ_c nominally increases with $3h'$. The dependence on interface thickness is more pronounced than the gradient 3D interface in a Nb matrix. The σ_c peaks and then plateaus when $3h'$ reaches 9.24 nm, which is nearly twice the limit h' of the monolayer interfaces of the same compositions. The plateau value, $0.04\mu_{Cu}$, however, is close to that of the monolayer $Cu_{0.9}Nb_{0.1}$ interface, the stronger composition. Again, we find that the barrier strength of the graded interface of two compositions is as strong as its stronger composition.

Figure 8b presents the sub-critical configurations of the L and T partials for the broad range of $3h'$ over which σ_c varies. From $3h' \approx$ 1–4 nm, when h' is less than the ISF width of the dislocation, σ_c enables L to cross the first two layers and into the final $Cu_{0.9}Nb_{0.1}$ layer while T lies in the first $Cu_{0.9}Nb_{0.1}$ layer. Evidently σ_c is needed to force L and T to glide across the two

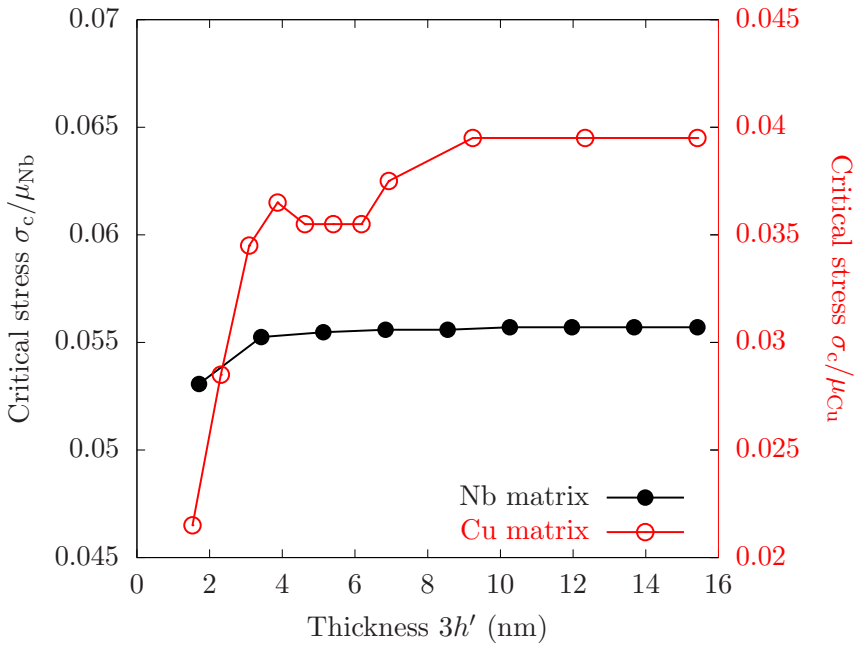

Figure 7. Critical stresses for transmission of an edge dislocation through the gradient interface in a Nb matrix or a Cu matrix, as a function of the total interface thickness.

stronger regions of the interface. The thicker h' these regions is, the greater the resistance. When $3h'$ increases above the ISF width from about 4 to 6 nm, however, σ_c still pushes L all the way into the last $Cu_{0.9}Nb_{0.1}$ layer but T lies in the weaker $Cu_{0.8}Nb_{0.2}$ layer. The σ_c decreases since achieving the critical configuration involves gliding through the weaker material. For greater $3h'$, σ_c reaches a limit value. The critical state at this limit corresponds to when the entire dislocation is on the verge of finally crossing the final interface/matrix boundary. The T partial has yet to transmit from the interface and back into the matrix (figure 8b at $3h' = 9.24$ nm).

4. Discussion

The results indicate a clear benefit in thickening the interface, where "larger is stronger" up to a limit thickness h'. These 3D interfaces can exhibit a non-negligible size effect on transmission resistance for thicknesses in the range of 2–10 nm. For some finely structured nanolaminates, these thicknesses are similar to or no smaller than the thickness of individual layers bounding the interfaces. With the added size effect from the interface h', altering both thicknesses independently to achieve optimal strength can be easily envisioned.

When treating a gradient interface, it is useful to consider the thickness of the composition within the interface that is the most resistant to glide. Calculations here forecast that rather than the weakest or even the averaged resistance across all compositions in the interface, it is the strongest portion of the interface and its volume fraction that dominates the resistance.

The dynamic, "composite" ISF width that transmits across the interface adds another important length scale. Although the resolved shear stresses on the L and T partials are the same, they often lie in different materials, differing in elastic moduli and lattice parameter. The results imply that greater differences in γ_{isf} between the matrix and 3D interface and lower γ_{isf} could possibly lead to even greater strengthening potential for 3D interfaces. Not only would the boosts in strengthening over the pure constituents be realized but also the range of h' could be greater than those seen in the composite system studied here.

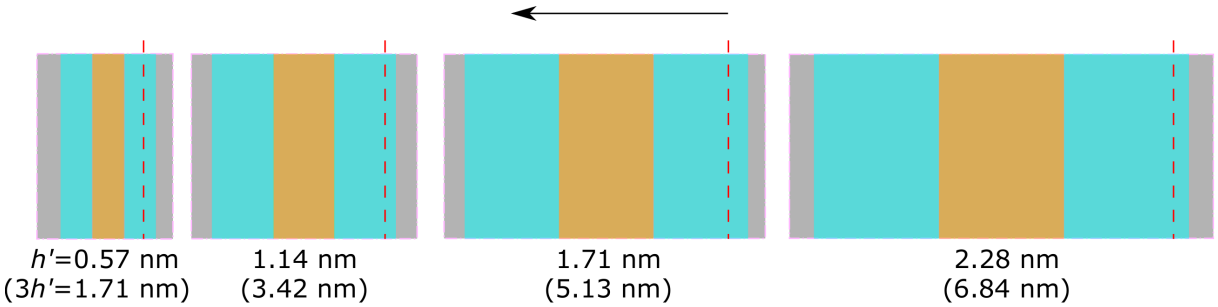

(a) Nb matrix

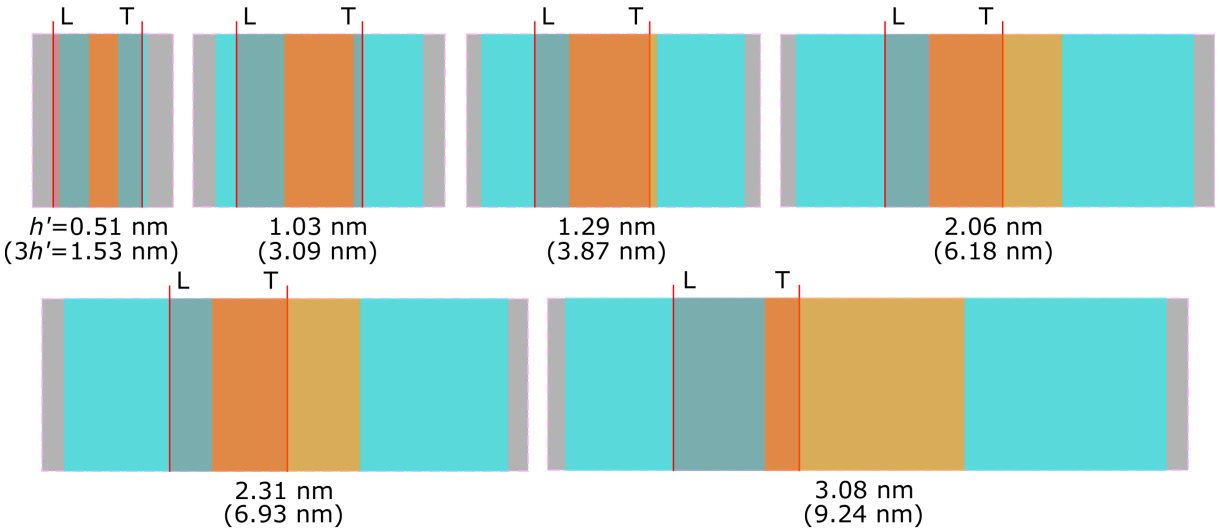

(b) Cu matrix

Figure 8. Position of the dissociated dislocation in their critical state, that is, when the applied stress is slightly lower than the critical one. Markers and parameters used are the same as those in figure 4 and figure 6.

5. Conclusions

In this paper, we utilize a recently developed multi-phase PFDD model [11] to study the transmission of an edge dislocation across compositionally gradient 3D interfaces of nanoscale thicknesses. The calculations investigate the role played by the 3D interface thickness h', composition, and dislocation core structure, either undissociated in BCC crystals or dissociated in FCC ones. One set-up consists of a fully BCC structure containing a thick 3D crystalline Cu-Nb alloy interface sandwiched between two Nb crystals of the same orientation. Similarly, the other one is composed of a completely FCC structure with two Cu crystals sharing one common thick 3D Cu-Nb alloy interface. Even for the finest h' ($\approx$ 0.5 nm), the interface increases the glide resistance, by 30–60% in the BCC structure and 40 times in the FCC one. For both crystal structures, a positive size effect in h' on transmission strength occurs up to a limit h' of $\approx$ 2–10 nm. We observe intrinsic stacking fault (ISF) strengthening, in which the dissociated core of the FCC dislocation leads to boosts in transmission strength over a broad range of nm thick interfaces. Comparisons with interfaces of uniform composition reveal that the transmission strength of gradient interfaces is controlled by its strongest composition. Thus, with the introduction of 3D interfaces, two important nm length scales arise, the thickness of the interface and the dynamic ISF width of the transmitting dislocation.

Acknowledgements
The authors gratefully acknowledge financial support from the Department of Energy, Office of Science, Basic Energy Sciences Program, USA DE-SC0020133. JYC is supported by DOE NNSA SSGF, USA under cooperative agreement number DE-NA0003960. Use was made of computational facilities purchased with funds from the National Science Foundation, USA (CNS-1725797) and administered by the Center for Scientific Computing (CSC), USA. The CSC is supported by the California NanoSystems Institute and the Materials Research Science and Engineering Center, USA (MRSEC; NSF DMR 1720256) at UC Santa Barbara.

References

[1] Mara N A and Beyerlein I J 2014 *J. Mater. Sci.* **49** 6497–516
[2] Mara N A and Beyerlein I J 2015 *Curr. Opin. Solid State Mater. Sci.* **19** 265–76
[3] Yang W, Beyerlein I J, Jin Q, Ge H, Xiong T, Yang L, Pang J, Zhou Y, Shao X, Zhang B, Zheng S and Ma X 2019 *Scr. Mater.* **166** 73–7
[4] Nizolek T, Beyerlein I J, Mara N A, Avallone J T and Pollock T M 2016 *Appl. Phys. Lett.* **108** 051903
[5] Pathak S, Velisavljevic N, Baldwin J K, Jain M, Zheng S, Mara N A and Beyerlein I J 2017 *Sci. Rep.* **7** 8264
[6] Han W Z, Cerreta E K, Mara N A, Beyerlein I J, Carpenter J S, Zheng S J, Trujillo C P, Dickerson P O and Misra A 2014 *Acta Mater.* **63** 150–61
[7] Zhang R F, Germann T C, Liu X Y, Wang J and Beyerlein I J 2014 *Acta Mater.* **79** 74–83
[8] Wang J, Zhang R F, Zhou C Z, Beyerlein I J and Misra A 2014 *Int. J. Plast.* **53** 40–55
[9] Chen Y, Li N, Hoagland R G, Liu X Y, Baldwin J K, Beyerlein I J, Cheng J Y and Mara N A 2020 *Acta Mater.* **199** 593–601
[10] Cheng J Y, Xu S, Chen Y, Li Z, Baldwin J K, Beyerlein I J and Mara N A 2022 *Nano Lett.* **22** 1897–904
[11] Xu S, Cheng J Y, Mara N A and Beyerlein I J 2022 *J. Mech. Phys. Solids* (under review)
[12] Li Z, Cheng J Y, Poplawsky J D, Xu S, Baldwin J, Beyerlein I J and Mara N A 2022 *Scr. Mater.* (under review)
[13] Xu S 2022 *Comput. Mater. Sci.* **210** 111419
[14] Xu S, Mianroodi J R, Hunter A, Svendsen B and Beyerlein I J 2020 *Int. J. Plast.* **129** 102689
[15] Xu S, Cheng J Y, Li Z, Mara N A and Beyerlein I J 2022 *Comput. Meth. Appl. Mech. Eng.* **389** 114426
[16] Xu S, Mianroodi J R, Hunter A, Beyerlein I J and Svendsen B 2019 *Philos. Mag.* **99** 1400–28
[17] Xu S, Smith L, Mianroodi J R, Hunter A, Svendsen B and Beyerlein I J 2019 *Modelling Simul. Mater. Sci. Eng.* **27** 074004
[18] Xu S, Su Y, Smith L T W and Beyerlein I J 2020 *J. Mech. Phys. Solids* **141** 104017
[19] Warlimont H and Martienssen W (eds) 2018 *Springer Handbook of Materials Data* 2nd ed (Springer International Publishing)
[20] Su Y, Xu S and Beyerlein I J 2019 *J. Appl. Phys.* **126** 105112
[21] Mianroodi J R, Hunter A, Beyerlein I J and Svendsen B 2016 *J. Mech. Phys. Solids* **95** 719–41